JCTC Journal of Chemical Theory and Computation

Article

pubs.acs.org/JCTC

Calculating CD Spectra of Flexible Peptides: An Assessment of TD-DFT Functionals

Zlatko Brkljača,[†] Momir Mališ,[‡] David M. Smith,*[,‡,§] and Ana-Sunčana Smith*[,†,‡]

[†]Institute for Theoretical Physics, Friedrich Alexander University Erlangen-Nürnberg, Staudtstrasse 7, Erlangen, 91058, Germany

[‡]Ruđer Bošković Institute, Bijenička 54, 10000, Zagreb, Croatia

[§]Center for Computational Chemistry, Friedrich Alexander University of Erlangen-Nürnberg, Nägelsbachstraße 25, Erlangen, 91052, Germany

Supporting Information

ABSTRACT: Calculations of CD spectra can provide important structural information for peptide systems. Although TD-DFT is an attractive method for these calculations, recent studies have pointed to problems with modeling charge transfer excitations. Motivated by these problems, we benchmarked the performances of CAM-B3LYP, ωB97X-D, M06-2X, B3LYP, and PBE0 against high level *ab initio* RICC2 calculations for selected peptide structures. Furthermore, we compared the performance of the functionals with the experimentally available data. Our results show that long-range corrected functionals (CAM-B3LYP and ωB97X-D) correlate relatively well with RICC2 calculations, as does the meta-hybrid M06-2X, while the global hybrid functionals (B3LYP and PBE0) exhibit the aforementioned charge-transfer artifacts. On the other hand, PBE0 and even more so M06-2X and B3LYP produce spectra in better agreement with the experimental data. We have clarified this apparent discrepancy by finding that the surplus charge-transfer excitations, exhibited by B3LYP and PBE0, seem to have a negligible contribution to the final spectra, once appropriate structural averaging is performed.

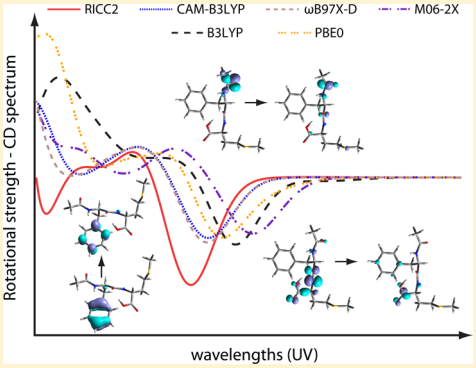

INTRODUCTION

Circular dichroism (CD) spectroscopy is one of the key experimental methods employed in the structural characterization of optically active chiral molecules. It is widely used in studies of biologically important systems, such as proteins. However, even though CD spectroscopy is very sensitive to the conformation of the studied proteins, its interpretation is usually based on the comparison of the CD spectrum of a protein of interest to a reference set consisting of CD spectra of proteins with known X-ray or NMR structures.[1] The quality of such an empirical approach strongly depends on the structural similarity between the protein of interest and the reference set. Approximate theoretical approaches have been successfully used to complement the experimental measurements and to correlate the molecular properties and spectral features, particularly in the case of proteins with well-defined secondary structures.[2−4]

CD spectroscopy has also been extensively applied to the structural characterization of peptides,[5,6] even though these species generally have less well-defined secondary structures. Thus, in this situation, theoretical methods also provide an attractive means to support the experiment and assign certain spectral features to specific structural motifs. However, for these flexible systems, obtaining a reliable theoretical description has proven to be a challenging task.[7]

In a recent study, we introduced a general methodology for calculating the CD spectra of flexible peptides.[8] In short (Scheme 1), the method is based on the generation of a converged conformational phase space, obtained from classical molecular dynamics simulations. A set of structures representing the entire phase space is then found using clustering analysis. The effects of the solvent are introduced through a modified average Coulomb field[9,10] for each conformation.[8] In the next step, an electronic structure method is chosen to calculate the individual CD spectra, which are subsequently

Scheme 1. Generalized Procedure for Calculating CD Spectra of a Flexible Molecule

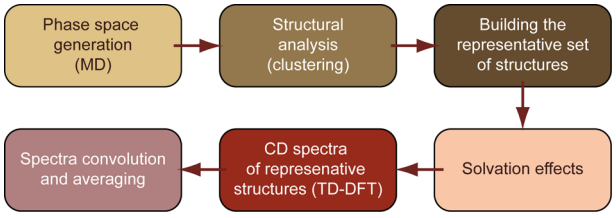

Received: January 30, 2014

   dx.doi.org/10.1021/ct500071t | J. Chem. Theory Comput. XXXX, XXX, XXX−XXX

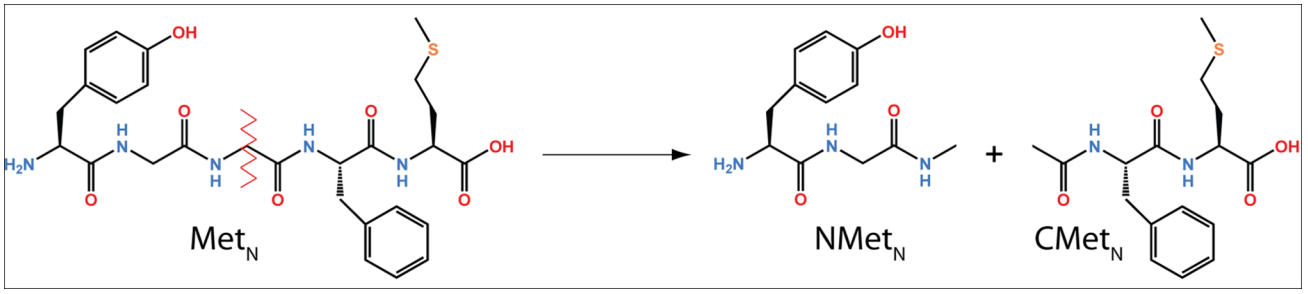

Figure 1. Neutral Met-enkephalin (Met_N) is shown on the left. Two neutral model peptides $NMet_N$ and $CMet_N$ are prepared by cutting along either the C_α(Gly3)−C_O(Gly3) or the C_α(Gly3)−N(Gly3) bond.

combined using appropriate weights to produce the final spectrum.

The choice of the electronic structure method is clearly an important component in the overall procedure. While semi-empirical methods have proven promising for certain classes of molecules,[11] including structured proteins,[2−4] this kind of approach has not been so successful in the case of flexible peptides.[7,12] *Ab initio* methods, such as the multireference[13,14] or coupled cluster methodologies,[15,16] would be expected to exhibit reliable accuracy. However, their computational cost and scaling properties render them tractable only for small peptide fragments.

A natural compromise between accuracy and cost for the calculation of peptide spectra is time-dependent density functional theory (TD-DFT). This approach has performed reasonably well in a number of applications,[17] ranging from metal complexes[18,19] to biologically important systems.[20−22] Nevertheless, implementations of TD-DFT may be associated with somewhat unpredictable precision,[23] particularly for larger systems.[20] In the context of electronic spectra calculations, TD-DFT is known to underestimate the excitation energies of transitions with a significant charge transfer (CT) character,[24−26] including those in peptide systems.[27] This problem stimulated the development of long-range corrected functionals (LCFs), including the relatively successful Coulomb-attenuated functional CAM-B3LYP[28] and the dispersion-encompassing ωB97X-D.[29] The hybrid meta GGA functional (HMF) M06-2X,[30] on the other hand, has been shown to predict CT transitions, with intermediate spatial overlap, with an accuracy similar to that of CAM-B3LYP.[26] Moreover, it was very recently shown that M06-2X provides reasonable excitation energies for a large set of conjugated molecules.[31] However, even the more traditional global hybrid functionals (GHFs), such as B3LYP[32] and to a lesser extent PBE0,[33] have proven quite accurate in some cases.[19,25,34] Indeed, recent extensive benchmarking studies found that the B3LYP functional often exhibits lower deviations from experimental results than, for example, CAM-B3LYP.[23,35] These conclusions have been recently generalized in an extensive review article.[36] Double hybrid approaches, such as TD-B2PLYP,[37] which combine TD-DFT with a CIS(D) type perturbation correction, have been found to offer some improvement over traditional functionals in terms of CD spectra.[38] However, due to their $\sim N^5$ scaling, these methods are not routinely applicable to larger and more flexible systems.[17]

In this work, we aim to investigate the performance of selected GHFs (B3LYP and PBE0), LCFs (CAM-B3LYP and ωB97X-D), and the HMF M06-2X for calculating CD spectra of peptides. As prototypical general peptides, we chose neutral and zwitterionic Met-enkephalin (Met_N and Met_Z),[8] which were further modified to obtain smaller model peptide systems. These smaller model systems were used to benchmark the performance of the functionals against the *ab initio* RICC2 method.[39,40] It should be noted that, despite its sophistication, the CC2 method is not infallible in terms of its predictions of excitation energies[41,42] and, in some cases, exhibits agreement with experimental data on a level similar to some TD-DFT functionals.[23,43] Nevertheless, the CC2 methodology can be expected to result in predictions free from DFT-related CT artifacts and to thus provide benchmark quality results in this respect.

In addition to the theoretical benchmarks, we also compare the performance of the functionals to the experimentally available data.[44] For this purpose, we calculated the average CD spectra of Met-enkephalin following the methodology outlined in our previous study.[8] Our results show that, for single conformations, the HMF and, even more so, the LCFs provide a satisfactory treatment of the excited state properties compared to the reference RICC2, while the GHFs fare somewhat poorer. Interestingly, the average CD spectra of Met-enkephalin calculated using the GHFs and especially B3LYP is in very good agreement with both M06-2X and the experimental spectrum. This implies that the averaging procedure substantially reduces the effects of the problems exhibited by the GHFs in the CD spectra of the individual model structures.

METHODS

Model Systems. The neutral model structures (Figure 1) were prepared from five Met_N conformations ($Tyr_0GlyGlyPheMet_0$, where the subscripted zero denotes neutral terminal residues), extracted from five clusters (I−V) of the phase space (Figure S1a) obtained in our previous study.[8] Each of the structures (Figure 2) was cut along the C_α(Gly3)−C_O(Gly3) bond or the C_α(Gly3)−N(Gly3) bond (shown in Figure 1). Capping the vacant positions with hydrogen atoms gives rise to the N-terminal model $NMet_N$

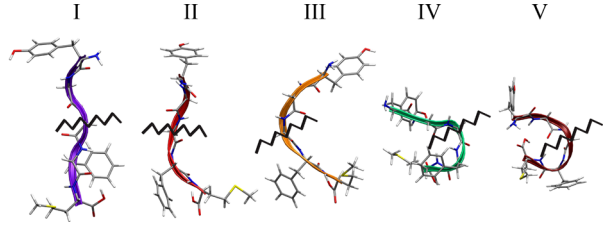

Figure 2. Five representative Met_N conformations plotted using the VMD visualization software.[45]

dx.doi.org/10.1021/ct500071t | J. Chem. Theory Comput. XXXX, XXX, XXX−XXX

($Tyr_0GlyNme$) and the C-terminal model $CMet_N$ ($AcePhe\text{-}Met_0$).

Zwitterionic models (Figure 3) of the C-terminus ($CMet_Z$) were prepared by cutting and capping five zwitterionic Met-

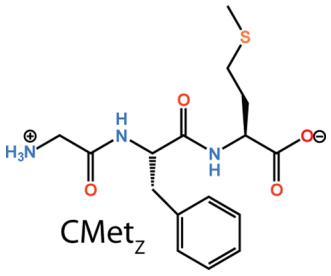

Figure 3. Zwitterionic model peptide structure ($CMet_Z$).

enkephalin structures (Met_Z, TyrGlyGlyPheMet), along the C_O(Gly2)-N(Gly3) bond. The original five structures were obtained from the conformational phase space of Met_Z (Figure S1b).[8]

Using parameters from the *ff*03[46] force field, supplemented with those previously developed for Tyr_0 and Met_0,[8] the CH_3 groups of the *N*-methyl (Nme in $NMet_N$) and acetyl (Ace in $CMet_N$) residues, as well as the NH_3^+ group of $CMet_Z$, were subjected to steepest descent minimization, while leaving the rest of the system frozen (Amber 10).[47] Thereby each model system was solvated with 226 molecules of TFE, using parameters from the RESP and ESP database.[48]

Excited State Calculations. The model systems were treated quantum mechanically, while the effects of the solvent were introduced through a modified implementation of the average solvent electrostatic configuration (ASEC) approach,[10] by spatially superimposing scaled charges from 50 uncorrelated solvent configurations (see Figures S2 and S3).[8] In the present applications, the solvent configurations were extracted every 10 ps from a series of 300 K NVT molecular dynamics simulations, with restrained solutes.

In the first instance, excitation energies and rotatory strengths were calculated using the RICC2 implementation in TURBOMOLE V6.3.1,[49] with TZVP[50] for both the atom-centered and the auxiliary basis sets. For comparison, TD-DFT calculations were performed with Gaussian 09,[51] using the CAM-B3LYP, ωB97X-D, M06-2X, B3LYP, and PBE0 functionals, in combination with either the 6-31G(d) or 6-311G(d,p) basis sets.

Using the calculated excitation energies and rotatory strengths, CD spectra were constructed by convoluting a series of state specific Gaussian functions of width σ = 0.135 eV, unless otherwise stated.

RESULTS

To properly asses the performance of the TD-DFT functionals, a state-by-state analysis is required. This analysis is presented in Tables 1 and 2 for $CMet_N$ and $NMet_N$, wherein the exited states are classified according to the dominant excitations in a given transition, using RICC2 as a reference. The wavelengths (Table 1) and rotatory strengths (Table 2) are obtained as averages over five $CMet_N$ and five $NMet_N$ structures, respectively. The standard deviations reflect the variation of the excitation energies and rotatory strengths, of a given transition, as a function of geometry. Any surplus states found in the TD-DFT calculations have been omitted from this analysis.

RICC2 Calculations. This method, chosen as the benchmark, predicts an average of seven excited states above 185 nm in the case of $CMet_N$, with four such states being found for $NMet_N$. The said states are organized in Tables 1 and 2, according to their characteristic average wavelength, in decreasing order. As can be seen from the standard deviations, the effects of geometry on the excitation energies are relatively small but may be more significant for the rotatory strengths.

A detailed inspection of the rotatory strengths in Table 2 reveals that, for $CMet_N$, there are three important transitions. The same transitions dominate the average CD spectrum, which is shown in Figure 4a. The most prominent transition is a C-terminal excitation at 220 nm (n_O(COOH) + π(F-M) →

Table 1. Average Wavelengths Together with Their Standard Deviations for Excited States in $NMet_N$ and $CMet_N$ (Lying above 185 nm) from the Values Obtained for Five Model Structures[a]

excited state[a]	wavelength / nm					
	RICC2	CAM-B3LYP	ωB97X-D	M06-2X	B3LYP	PBE0
tyrosine ^1L_b	259.2 ± 1.6	242.2 ± 1.4	242.4 ± 1.4	238.9 ± 1.4	250.1 ± 1.5	245.9 ± 1.5
phenylalanine ^1L_b	243.4 ± 0.6	227.8 ± 0.8	227.9 ± 0.7	225.5 ± 0.8	233.5 ± 0.7	229.4 ± 0.6
n_O(COOH) + π(F-M) → π^*(COOH)	219.1 ± 0.6	223.3 ± 0.9	222.9 ± 0.9	233.0 ± 0.8	228.3 ± 1.6	225.5 ± 0.4
n_S(M) → n_S(M)*	213.0 ± 1.9	216.7 ± 2.3	215.6 ± 2.3	224.9 ± 2.3	222.2 ± 3.1	217.9 ± 3.4
n_O(Y) → π^*(Y-G)	212.5 ± 1.3	214.7 ± 1.3	214.3 ± 1.4	221.6 ± 1.1	220.4 ± 1.2	213.3 ± 4.2
n_O(F) → π^*(F-M)	210.8 ± 3.7	210.8 ± 3.8	210.7 ± 3.5	217.6 ± 4.0	221.1 ± 3.5	213.3 ± 2.8
n_O(G) → π^*(G-Nme)	205.8 ± 2.4	209.3 ± 2.3	208.7 ± 2.4	216.2 ± 2.2	213.7 ± 3.3	210.6 ± 2.8
n_O(Ace) → π^*(Ace-F)	205.4 ± 2.1	208.3 ± 1.9	207.7 ± 1.9	214.8 ± 2.2	212.8 ± 2.0	209.7 ± 2.0
tyrosine ^1L_a	203.1 ± 0.8	206.6 ± 0.8	206.0 ± 0.7	201.7 ± 0.8	212.1 ± 0.5	212.1 ± 2.8
phenylalanine ^1L_a	193.3 ± 0.5	201.2 ± 0.7	200.7 ± 0.7	195.6 ± 0.9	208.8 ± 1.1	204.6 ± 1.4
n_S(M) → π^*(COOH)	188.8 ± 2.1	191.5 ± 7.6	189.2 ± 7.3	193.0 ± 7.2	259.5 ± 12.4	244.3 ± 10.4

[a]Colors are used for clarity. The states are ordered according to the average wavelength obtained by RICC2. [b]The single capital letters are used to denote the amino acids. The sequence of $CMet_N$ and $NMet_N$ in this notation would thus be written as Ace-F-M and Y-G-Nme, respectively. Aromatic excitations are denoted using the standard nomenclature. Orbitals of the π type of the amide bond between Phe and Met are denoted as π(F−M). Lone pairs are denoted as n with their elemental symbol subscripted. Thus, n_O(Ace) refers to a nonbonding orbital on the carbonyl oxygen of acetyl residue; n_S(M) is a nonbonding orbital on the sulfur atom of the Met side chain, while n_O(COOH) is a nonbonding orbital on the carbonyl oxygen of the C-terminal carboxylic acid group. Antibonding orbitals are denoted with an * in the standard manner (the exception is n_S(M)*, which denotes an unoccupied orbital). The principle transitions are shown graphically in Table S2.

dx.doi.org/10.1021/ct500071t | J. Chem. Theory Comput. XXXX, XXX, XXX−XXX

Table 2. Rotatory Strengths Together with Their Standard Deviations for Excited States in $NMet_N$ and $CMet_N$ (Lying above 185 nm) from the Values Obtained for Five Model Structures[a]

excited state[a]	rotatory strength /10^{-40} erg esu cm gauss^{-1}					
	RICC2	CAM-B3YLP	ωB97X-D	M06-2X	B3LYP	PBE0
tyrosine ^1L_b	6.1 ± 9.0	7.9 ± 14.1	7.4 ± 13.1	8.7 ± 14.8	7.6 ± 14.6	7.8 ± 14.4
phenylalanine ^1L_b	0.1 ± 0.3	0.7 ± 0.9	0.6 ± 0.8	1.2 ± 2.0	0.2 ± 1.5	1.2 ± 1.8
n_O(COOH) + π(F-M) → π^*(COOH)	-31.0 ± 7.6	-18.9 ± 6.2	-20.2 ± 6.5	-18.2 ± 5.7	-23.1 ± 7.6	-16.6 ± 9.7
n_S(M) → n_S(M)*	0.3 ± 0.9	1.2 ± 2.7	1.5 ± 2.7	1.4 ± 2.5	3.3 ± 6.3	1.7 ± 2.7
n_O(Y) → π^*(Y-G)	10.5 ± 8.0	7.4 ± 7.3	7.9 ± 6.9	3.7 ± 5.9	8.3 ± 7.0	10.6 ± 3.4
n_O(F) → π^*(F-M)	7.5 ± 9.5	7.3 ± 8.9	4.1 ± 10.2	6.7 ± 9.0	7.9 ± 13.9	8.4 ± 14.8
n_O(G) → π^*(G-Nme)	-3.2 ± 7.6	-5.8 ± 8.7	-4.7 ± 7.5	-2.9 ± 5.0	1.0 ± 3.7	-6.4 ± 10.6
n_O(Ace) → π^*(Ace-F)	0.6 ± 4.5	-0.4 ± 2.2	0.6 ± 3.2	0.6 ± 2.9	-1.7 ± 3.8	-2.6 ± 4.1
tyrosine ^1L_a	1.0 ± 22.1	3.8 ± 25.3	1.4 ± 22.6	3.7 ± 28.9	1.9 ± 12.7	4.4 ± 8.6
phenylalanine ^1L_a	3.2 ± 8.1	3.2 ± 2.5	3.7 ± 2.8	3.0 ± 4.8	3.5 ± 9.2	6.4 ± 14.7
n_S(M) → π^*(COOH)	-13.1 ± 20.3	-6.3 ± 8.9	-11.6 ± 14.6	-1.6 ± 4.6	-0.7 ± 1.8	-4.2 ± 6.4

[a]Colors are used for clarity. The states are ordered according to the average wavelength obtained by RICC2.

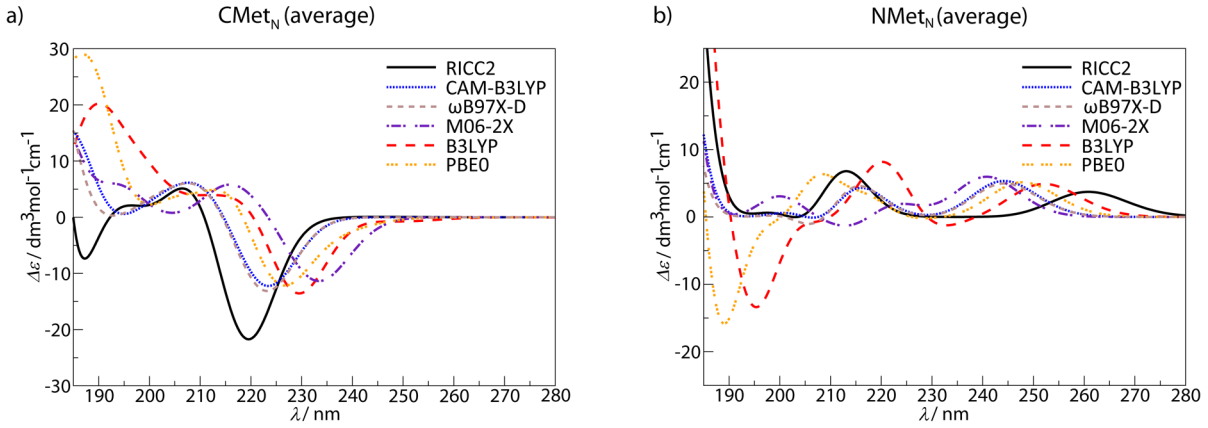

Figure 4. CD spectra averaged over five structures of (a) $CMet_N$ and (b) $NMet_N$.

π^*(COOH)), which exhibits a strongly negative rotatory strength and thus results in a deep minimum in the CD spectrum. A small maximum, which originates from the n_O(F) → π^*(F-M) amide transition, is evident at 210 nm. A second transition involving the C-terminal carboxylic group (188 nm, n_S(M) → π^*(COOH)) is also associated with a negative average rotatory strength, which is manifested in the spectrum as a small minimum at low wavelengths. This transition is associated with a nonlocal (CT) character and is subject to a relatively large variation in wavelength in response to changes in geometry, as evidenced by the corresponding standard deviation (especially with TD-DFT). At even shorter wavelengths, RICC2 identifies additional states with CT character, out of which the π (F) → π^*(COOH) transition at 180 nm has a relatively significant, positive average rotatory strength. Due to the broadening of the spectral lines, this transition may affect the theoretical spectra at wavelengths that are experimentally accessible (>185 nm).

In the case of $NMet_N$, there are two dominant transitions that result in two positive peaks in the CD spectrum (Figure 4b). These peaks are associated with an amide transition at 212 nm (n_O(Y) → π^*(Y-G)) and the aromatic tyrosine L_b transition at 259 nm. The latter also exhibits the highest wavelength observed in all the studied model systems.

Experimentally, the tyrosine L_b transition occurs at around 275 nm,[52,53] meaning that RICC2 underestimates its wavelength by some 15 nm. Similar deviations are observed for the wavelengths of the phenylalanine L_b and L_a transitions, which are measured at 260 and 210 nm,[53] respectively. The wavelength for the tyrosine L_a state (λ_{exp} = 230 nm), on the other hand, is underestimated by RICC2 by approximately 25 nm. These deviations point to some systematic discrepancies in the prediction of energies of aromatic transition by RICC2, also noticed previously.[54]

Long-Range Corrected Functionals. The behaviors of the two LCFs considered in the present application (CAM-B3LYP and ωB97X-D) are remarkably similar (Figure 4). For example, above 185 nm, both LCFs predict an average of between seven and eight states for $CMet_N$, and four states for $NMet_N$ (Table S1), which is also in good agreement with RICC2. Similarly, the LCFs are the only functional class that completely reproduces the ordering of the states predicted by RICC2 (compare columns two to four in Table 1). Furthermore, the LCFs exhibit the best overall agreement with the average transition wavelengths of the reference calculations, while the rotatory strengths are reasonably well reproduced. The agreement with RICC2 is particularly good in the case of the C-terminal excitation (~220 nm) that dominates the $CMet_N$ spectrum, as well as with the amide transitions. The latter is reflected in the similarities of the average CD spectra, particularly with respect to amide-type transitions. However, in the comparison with both RICC2 and the experiment, the LCFs perform relatively poorly for the aromatic L_b transitions, shifting them to considerably lower wavelengths. This can be seen, for example, in the misplaced second maximum in the average $NMet_N$ spectrum (Figure 4b).

dx.doi.org/10.1021/ct500071t | J. Chem. Theory Comput. XXXX, XXX, XXX−XXX

Despite these deviations, one can conclude that both LCFs exhibit nearly quantitative agreement with RICC2, a finding further supported by a very recent benchmarking study.[35] This conformity is not only apparent on the level of the average transitions and spectra but also on the level of single structures, as shown in Figure 5.

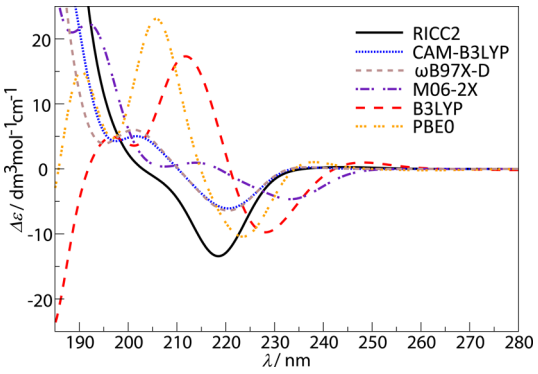

Figure 5. Example CD spectra of a single structure of $CMet_N$.

The Hybrid Meta Functional. M06-2X performs similarly to the LCFs in terms of its comparison with RICC2. This is particularly true with respect to the number of states (Table S1) and their rotatory strengths (Table 2). However, larger deviations are obtained for the transition wavelengths, and in some cases, the order of the states is inverted (compare the second and fifth columns in Table 1). Most nonaromatic transitions, including those with CT character, are subject to a relatively consistent but not entirely systematic red shift of around 10 nm. This is most visible in the positions of the dominant spectral features above 200 nm in the $CMet_N$ average spectrum, as well as in the position of the nearly lost maximum associated with the amide transition in the $NMet_N$ average spectrum (Figure 4). The performance of the HMF for the L_b transitions is similar to that of the LCFs although the former compares better than the latter to RICC2 for the L_a transitions. On the whole, the M06-2X functional reproduces the majority of the key elements of the transitions and spectra predicted by RICC2, but due to the larger deviations in wavelengths, the agreement remains qualitative.

Global Hybrid Functionals. The B3LYP and PBE0 functionals typically overestimate the number of excited states for the systems studied herein. For example, in the case of $CMet_N$, B3LYP and PBE0 find about 25 and 20 states, respectively, in the same wavelength region where RICC2 predicts seven (Table S1). This difference between the two GHFs is to be expected and stems from the fact that the higher proportion of exact exchange present in PBE0 leads to less artificially created excited states than for B3LYP.[38] Otherwise, however, the two GHFs exhibit a relatively high degree of mutual agreement, with the caveat that many of the PBE0 transitions tend to be somewhat blue-shifted relative to B3LYP. This has the effect of a relatively uniform leftwards displacement of the average PBE0 spectra in Figure 4, with respect to their B3LYP counterparts. From all the functionals tested, B3LYP has the smallest deviations from RICC2 in terms of wavelengths for the aromatic L_b transitions (also seen in the average spectrum of $NMet_N$). At the same time, the GHF L_a transitions are relatively strongly red-shifted with respect to RICC2, bringing them closer to the experimental values. The nonaromatic transitions calculated by the GHFs follow most closely the M06-2X results and therefore appear at longer wavelengths than the RICC2 results. The exception is the CT transition ($n_S(M) \rightarrow \pi^*(COOH)$) that is significantly overstabilized by the GHFs, but its contribution to the overall rotatory strength at large wavelengths becomes small after averaging over five structures, especially for B3LYP.

The majority of the surplus states, found by the GHFs but not by RICC2 or the other functionals, appear at wavelengths shorter than 210 nm and are typically associated with a nonlocal (CT) character. The main consequence of these states is the qualitative disagreement with RICC2 in the spectra of single structures, particularly in the range of wavelengths below 210 nm (see, for example, Figure 5). Further inspection of the rotatory strengths of the surplus transitions suggests that their contribution is small and sporadic, although numerous. Hence, it is only natural that their impact on the average spectrum diminishes with increasing the number of considered structures. As a result, the performance of both GHFs improves significantly upon averaging (Figure 4).

Zwitterionic Forms. The occurrence of CT artifacts in TD-DFT could be expected to be even more prominent in zwitterionic systems. To evaluate these effects in the context of our study, we compare the average spectrum of the $CMet_Z$ structures obtained with RICC2 to the TD-DFT functionals (Figure 6). Interestingly, the results are consistent with those

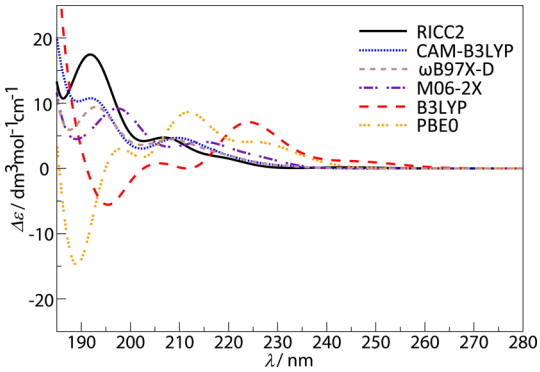

Figure 6. Average CD spectra of five structures of $CMet_Z$.

obtained for the neutral structures. Both the LCFs and the MHF agree with RICC2 in the number of predicted excitations (Table S1). The spectra predicted by LCFs reproduce the RICC2 excitation energies well, although the rotatory strengths appear weaker. M06-2X shows very similar rotatory strengths to LCFs, but the excitation energies are red-shifted, albeit to a lesser extent than in the neutral system. B3LYP and, to a lesser extent, PBE0 deviate even more in terms of the average number of predicted excitations (Table S1), and again, larger deviations from the benchmark curve can be seen. However, even in these cases, the performance of the GHFs improves significantly upon averaging.

Additivity of $NMet_N$ and $CMet_N$. It is interesting to consider to what extent the sum of the spectra of the two peptide fragments (Figure 1) compare to the spectrum of Met_N. We perform this analysis on the example of the averaged $NMet_N$ and $CMet_N$ spectra, calculated with CAM-B3LYP (Figure 4), and show (Figure 7) that their sum exhibits the same key features as the spectrum arising from averaging over the corresponding five full structures of Met_N (Figure 2).

dx.doi.org/10.1021/ct500071t | J. Chem. Theory Comput. XXXX, XXX, XXX−XXX

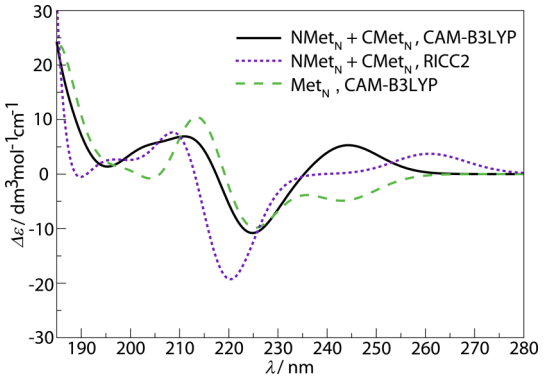

Figure 7. Superposition of average NMet$_N$ and CMet$_N$ spectra (CAM-B3LYP, black solid line; RICC2, violet dotted line) are compared to the average CD spectrum of the corresponding five Met$_N$ structures (CAM-B3LYP, green dashed line).

Because of the size of Met$_N$, it is difficult to perform the analogous comparison with the RICC2 approach. Interestingly, however, there is a reasonable agreement between the averaged spectrum of Met$_N$ calculated with CAM-B3LYP and the spectrum that is obtained from the sum of the fragment spectra obtained with RICC2. On this basis, it is plausible to expect that, in this specific case, the RICC2 spectra of Met$_N$ would resemble the CAM-B3LYP spectra of Met$_N$ shown in Figure 7. This presumption is supported by the quantitative analysis presented in the previous section but, due to the differing size dependence of the two methods, is not expected to hold either rigorously or generally.

Basis Set Dependence. Using the spectrum arising from averaging over the five full structures of Met$_N$ (Figure 2, as for the green-dashed line in Figure 7), we have investigated the effect of using a larger basis set in the evaluation of the Met$_N$ CD spectra. The corresponding analysis for each of the five chosen functionals is presented in Figure 8. Inspection of these results immediately reveals the high degree of similarity between the 6-31G(d) and 6-311G(d,p) spectra. The only functional that exhibits any significant basis-set-related deviations is B3LYP and only then at wavelengths shorter than 210 nm. As previously mentioned, many of the states in this region are associated with a nonlocal character and their impact becomes less significant with greater averaging. This behavior is confirmed in Figure S4, which shows that the Met$_N$ spectra obtained using TD-B3LYP/6-311G(d,p) and all 50 representative structures are very similar to that obtained under the same conditions with the 6-31G(d) basis set. Overall, it seems the results obtained with the 6-31G(d) set are a good approximation to those emerging from the use of the larger 6-311G(d,p). This lends confidence to the continued use of 6-31G(d), as we have done in the subsequent sections.

Met$_N$. To further investigate the performance of the TD-DFT functionals, we performed an analysis of the underlying excitations and constructed the average CD spectra of Met$_N$, from 50 structures that were representative of the entire conformational space.[8] We compare these calculations to the experimentally obtained spectrum[44] (Figure 9) using the fact that, in TFE, the neutral form of the peptide (Met$_N$) is expected to dominate. The zwitterionic form (Met$_Z$) is estimated to account for 10% of the N:Z equilibrium[8] and therefore to have only a minimal impact on the combined spectra, which are shown in the SI (Figure S5).

As opposed to the purely theoretical analysis of the model systems performed in the previous section, the quality of the comparison with experimental data is dependent on the ability of the overall approach (Scheme 1) to capture the variations of the solvent and the structure of the peptide in solution. Although these issues are addressed in detail in ref 8, we have included a brief summary here. The appropriateness of our implementation of a modified ASEC approach is established by comparison with a brute-force alternative that evaluates and combines the spectra associated with numerous individual solvent configurations (Figure S3). The number and choice of individual (solvent-averaged) peptide structures, used to construct the overall spectra, is based on our previous analysis of convergence within and across selected clusters,[8] whereas Figure S7 compares alternative sampling options. While our chosen approaches for both solvent and structural averaging

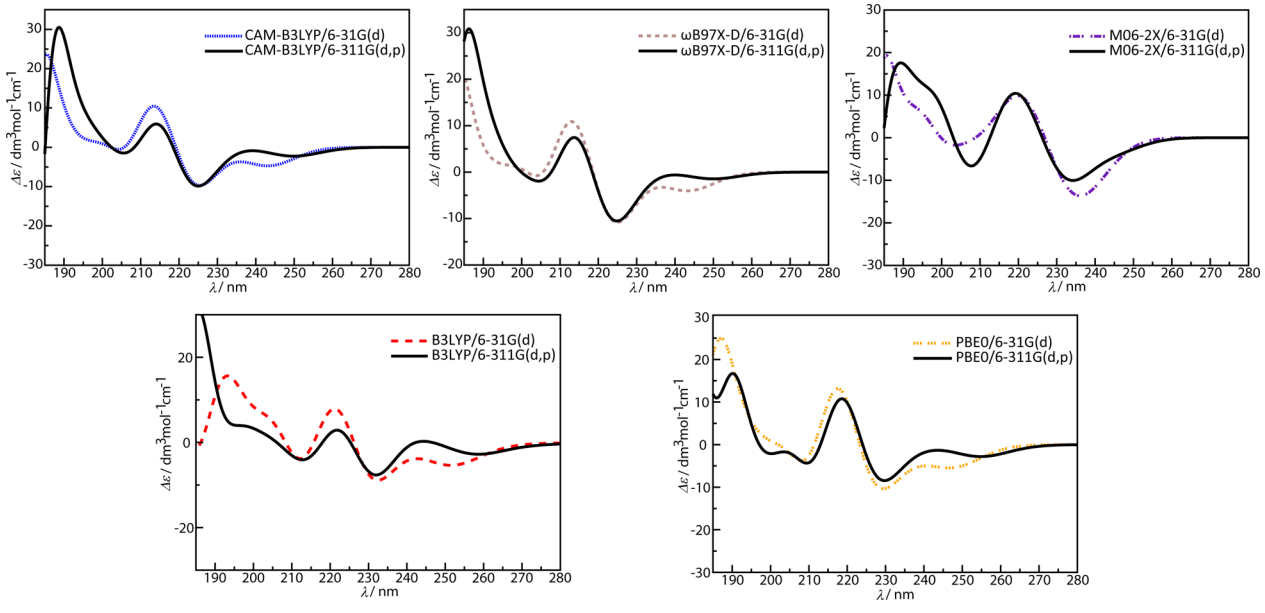

Figure 8. Basis set dependence of the CD spectra arising from averaging over the corresponding five full structures of Met$_N$ (Figure 2).

dx.doi.org/10.1021/ct500071t | J. Chem. Theory Comput. XXXX, XXX, XXX−XXX

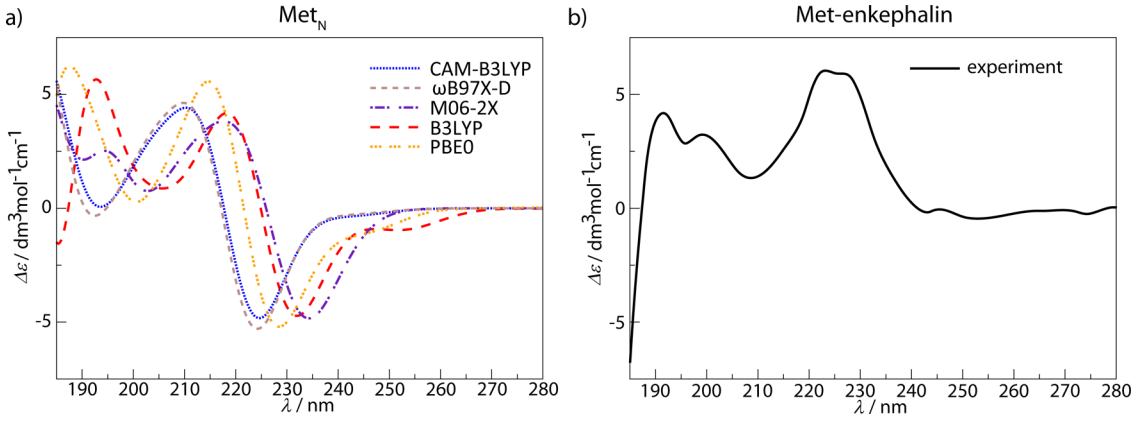

Figure 9. (a) Theoretically calculated CD spectra of Met_N. (b) Experimentally obtained CD spectrum of Met-enkephalin in TFE.[44]

are, by definition, approximations, we believe that they exhibit sufficient convergence to serve as a solid basis for the present analysis of the ability of different TD-DFT functionals to capture the main spectral features.

Consequently, we calculate the CD spectrum of Met_N for all five functionals, and the results are shown, together with the experimental spectrum,[44] in Figure 9. Overall, we find very good agreement between B3LYP and M06-2X, as well as a reasonable correspondence of these two functionals with the experimental CD spectrum. The PBE0 spectrum for Met_N closely parallels that of B3LYP, but as was the case for the model structures, it is marginally but relatively uniformly shifted toward lower wavelengths. The spectra obtained with CAM-B3LYP and ωB97X-D once again exhibit practically identical behavior. Although the LCF spectra exhibit the same general features as the other functionals, they are blue-shifted by approximately 10 nm, a result which is also consistent with those obtained for the smaller model structures.

The only larger discrepancy between all the calculated spectra and the experiment is the strong minimum between 230 and ∼235 nm seen in the M06-2X and B3LYP spectra, just below 230 nm for PBE0 and at ∼224 nm for CAM-B3LYP and ωB97X-D (Figure 9a). This minimum is induced by the dominant n_O(COOH) + π(F-M) → π^*(COOH) excitation, also appearing in $CMet_N$ (Figure 4a). The resemblance of the CAM-B3LYP and RICC2 spectra (Figure 7), as well as the systematic appearance of this transition with even more negative rotatory strengths within the RICC2 approach (Tables 1 and 2), suggests that this transition is not unique to TD-DFT. Furthermore, since this transition only arises for neutral peptides, one could imagine that the contribution of the zwitterionic form to the experimental spectra is larger than expected. However, the superposition of the Met_Z and Met_N spectra with zwitterionic fractions larger than 10% does not improve the overall comparison with experiments. This is true for all the functionals (Figure S5), even though at least M06-2X and the LCFs do not appear to suffer from CT artifacts when applied to (C)Met_Z (average CD spectra of Met_Z are shown in Figure S6). On the basis of these considerations, we are confident to conclude that the persistent appearance of the n_O(COOH) + π(F-M) → π^*(COOH) excitation is not related to the TD-DFT approach and its potential difficulties with charge-transfer transitions.

The strongest correspondence between the theoretical and the experimental spectra is in the peak measured at ∼220 nm. With M06-2X and B3LYP, it also appears at ∼220 nm, while PBE0 and the LCFs center it, less accurately, closer to 210 nm. This maximum corresponds to the combination of two amide n → π^* excitations, namely n_O(Y) → π^*(Y-G) and n_O(F) → π^*(F-M), which were also the dominant excitations in $NMet_N$ and $CMet_N$, respectively (Tables 1 and 2). Between this and the adjacent peak, all five spectra remain positive, with minima appearing at 205, 203, 200, 193, and 192 nm, for B3LYP, M06-2X, PBE0, CAM-B3LYP, and ωB97X-D, respectively. The corresponding minimum in the overall positive experimental CD spectrum lies at ∼208 nm.

The next prominent feature in the experimental spectrum is the positive peak centered at around ∼195 nm. Although this wavelength borders on the edge of the window for reliable measurements and may hence be accompanied by a minimally accentuated uncertainty, it is nevertheless instructive to consider the behavior of the TD-DFT functionals in this region. Both the B3LYP and M06-2X spectra exhibit a positive peak at around the correct wavelength, while the analogous PBE0 feature is again blue-shifted. A similar but broader maximum is found for the LCFs between 175 and 190 nm, which is indeed below the wavelengths accessed in the discussed experiments. A more detailed analysis of excitations in the CAM-B3LYP and ωB97X-D peaks over all 50 structures reveals that the dominant contributions come from local π(Y) → π^*(Y) transitions (which potentially represent the low frequency tail of the B_a and B_b excitations) and, to a lesser extent, from various π/n_O(amide) → π^*(amide) transitions. Despite the long-range corrections inherent to these functionals, we furthermore find numerous transitions with a strong CT character in this wavelength range. The most common are excitations of the type π/n_O(amide) → π^*(aromatic) and π(aromatic) → π^*(amide), as well as n_S(M) → π^*(amide) and n_s(M) → π^*(F).

Guided by the assignments of excitations from the LCF spectra, we analyzed the excitations contributing to the peaks observed in the B3LYP and PBE0 spectra around 195 and 190 nm, respectively. Despite the occurrence of many more CT transitions with the GHFs, the overall conclusions regarding the identification of the key contributors are virtually identical to those outlined above for the LCFs. Importantly, however, the overall spectral feature produced by B3LYP (and to a lesser extent PBE0) is more consistent with the experiment than that arising from CAM-B3LYP and ωB97X-D. Interestingly, B3LYP is the only functional that exhibits the same behavior as the experimental spectrum in the lowest wavelength region (below 190 nm) following the maximum at 195 nm, although, as

dx.doi.org/10.1021/ct500071t | J. Chem. Theory Comput. XXXX, XXX, XXX−XXX

Table 3. Mean Signed Errors (MSE) of TD-DFT Transition Wavelengths from RICC2 Values Calculated as $(1/n)\sum_i \mathrm{TDDFT}_i - \mathrm{RICC2}_i$[a]

excitation type	excited state	wavelength / nm				
		CAM-B3LYP	ωB97X-D	M06-2X	B3LYP	PBE0
aromatic excitations	tyrosine ^1L_b	-17.0	-16.8	-20.3	-9.1	-13.3
	phenylalanine ^1L_b	-15.6	-15.6	-17.9	-9.9	-14.0
	tyrosine ^1L_a	3.4	2.8	-1.4	8.8	8.8
	phenylalanine ^1L_a	7.9	7.4	2.4	15.4	11.3
CT	$n_S(M) \rightarrow \pi^*(COOH)$	5.7	3.2	7.1	74.8	59.0
amide excitations	$n_O(Y) \rightarrow \pi^*(Y\text{-}G)$	2.2	1.8	9.2	8.0	1.1
	$n_O(F) \rightarrow \pi^*(F\text{-}M)$	0.0	-0.1	6.8	9.3	2.5
	$n_O(G) \rightarrow \pi^*(G\text{-}Nme)$	3.5	2.9	10.4	8.0	4.8
	$n_O(Ace) \rightarrow \pi^*(Ace\text{-}F)$	2.9	2.3	9.4	7.4	4.3

[a]TDDFT_i and $\mathrm{RICC2}_i$ correspond to the values of the wavelength of the particular excitation in the ith peptide model found using the TD-DFT method of interest and RICC2, respectively.

Table 4. Mean Signed Errors (MSE) of TD-DFT Transition Rotatory Strengths from RICC2 Values Calculated as $(1/n)\sum_i \mathrm{TDDFT}_i - \mathrm{RICC2}_i$[a]

excitation type	excited state	rotatory strength /10^{-40} erg esu cm gauss^{-1}				
		CAM-B3LYP	ωB97X-D	M06-2X	B3LYP	PBE0
aromatic excitations	tyrosine ^1L_b	1.8	1.3	2.6	1.6	1.8
	phenylalanine ^1L_b	0.6	0.5	1.1	0.1	1.1
	tyrosine ^1L_a	2.8	0.4	2.6	4.9	7.5
	phenylalanine ^1L_a	0.0	0.5	0.8	-3.5	3.2
CT	$n_S(M) \rightarrow \pi^*(COOH)$	10.0	7.1	12.0	12.9	11.7
amide excitations	$n_O(Y) \rightarrow \pi^*(Y\text{-}G)$	-3.2	-2.6	-6.8	-0.5	5.6
	$n_O(F) \rightarrow \pi^*(F\text{-}M)$	-0.2	-3.4	-0.9	1.8	0.9
	$n_O(G) \rightarrow \pi^*(G\text{-}Nme)$	-2.7	-1.6	0.3	0.6	-3.2
	$n_O(Ace) \rightarrow \pi^*(Ace\text{-}F)$	-1.0	0.0	0.0	-2.3	-3.1

[a]TDDFT_i and $\mathrm{RICC2}_i$ correspond to the values of the rotatory strength of the particular excitation in the i-th peptide model found using the TD-DFT method of interest and RICC2, respectively.

mentioned earlier, the uncertainties in the experimental curve are expected to increase at these lower wavelengths.

The M06-2X functional, on the other hand, gives the ratio of the average rotatory strengths for the two dominant peaks in the overall spectrum (Figure 9a) most similar to that in the experiment. With this functional, however, the peak at 195 nm is associated with the phenylalanine L_a excitation (average rotatory strength of $\sim 5 \times 10^{-40}$ erg esu cm Gauss^{-1}), coupled with a small contribution from the $n_S(M) \rightarrow \pi^*(COOH)$ excitation, consistent with the result over five structures (Table 1). This is despite the fact that the rotatory strengths of the L_b and L_a aromatic transitions, averaged over all 50 structures, are negligible, for all other investigated functionals. For example, B3LYP predicts the phenylalanine L_a excitation at ~206 nm, and with an average rotatory strength close to zero.

It should be noted that, relative to the HMF and LCFs, the GHFs frequently overstabilize CT transitions which then appear over the entire wavelength range of interest. A typical example is the $n_S(M) \rightarrow \pi^*(COOH)$ transition, which, with B3LYP, appears with an average wavelength of 253.4 nm and a mean rotatory strength of -0.25×10^{-40} erg esu cm Gauss^{-1} (over 50 structures). This is even closer to zero than after averaging over five structures (Table 2). Such a trend, where the impact of spurious CT excitations tends to vanish after averaging over a sufficient number of structures, seems to apply quite generally.

DISCUSSION

While modeling the CD spectra of flexible molecules is the only possible way to associate the measured spectra with their conformational phase spaces, the current and previous[8] work clearly demonstrates the complexity of this task. The helpful fact here is that, irrespective of the choice of the method, the relevant transitions and their excitation energies depend only weakly on the choice of peptide conformation. On the other hand, the rotational intensity of these excitations may change significantly with the peptide configuration. Since the measured signal contains contributions from all possible conformations, to correctly reproduce the experimental spectrum, appropriate averaging over theoretical spectra from a number of structures must be performed.[8]

The effect of averaging is perhaps best seen in the comparison of the Met_N spectra shown in Figures 7 and 9, where the averaging is performed over a set of 5 and 50 structures, respectively. In the former case, one of the dominant features of the spectrum is the tyrosine L_b peak at longer wavelengths. However, after appropriate averaging, the contribution of this excitation becomes negligible. This is also generally true for the intensity of the two local phenylalanine transitions. Interestingly, on the level of a single structure, these excitations are associated with small rotatory strengths while the tyrosine transitions appear to be very sensitive to the

dx.doi.org/10.1021/ct500071t | J. Chem. Theory Comput. XXXX, XXX, XXX−XXX

geometry, leading to the notably large standard deviations (see Table 2).

In the context of using RICC2 calculations as a benchmark for the TD-DFT approach (Tables 3 and 4 and Tables S3 and S4), both the tyrosine and phenylalanine L_b transitions are blue-shifted for all investigated functionals (first two rows in Table 3). Nevertheless, the excitation energies predicted by B3LYP for these transitions agree best with RICC2, while M06-2X disagrees most. On the contrary, L_a transitions predicted with TD-DFT are typically red-shifted, with B3LYP deviating most from RICC2, while M06-2X shows nearly quantitative agreement. Interestingly, the sensitivity of the rotatory strength to the peptide conformation is also reflected in the comparison between high and low accuracy approaches. Thereby, TD-DFT relatively accurately reproduces the rotatory strengths predicted by RICC2 for phenylalanine transitions, but the deviations are significantly larger for tyrosine excitations, particularly with B3LYP (compare the first four rows in Table 4).

From the perspective of the experimentally available results, which indicate a blue shift for all aromatic transitions predicted by RICC2, one can conclude that TD-DFT is inferior to the higher-level approach when L_b transitions are considered but that it performs better for L_a transitions. A natural extension of the above conclusion is that B3LYP outperforms the other functionals in modeling aromatic transitions, especially in terms of their excitation energies (see also refs 23, 31, and 35). This is particularly important when assessing the reliability of the maximum[31] associated with the phenylalanine L_a transition, predicted only by M06-2X at 195 nm, in the spectrum of Met_N.

The comparison of TD-DFT with RICC2 is especially useful for nonlocal transitions involving charge transfer, even though the direct comparison with experiments is currently challenging. In the case of the systems studied herein, RICC2 predicts one principle transition of this type ($n_S(M) \rightarrow \pi^*(COOH)$) in the wavelength range of interest (>185 nm). This same transition is also found by TD-DFT. For CAM-B3LYP, ωB97X-D, and M06-2X, it appears at somewhat larger, but relatively similar, wavelengths (fifth row in Table 3). For B3LYP and PBE0, the red shift is considerably more pronounced.

Thus, although it can be expected for the TD-DFT approaches to exhibit artificial or overstabilized CT excitations, we find these to be prominent only for the GHFs in the considered energy range. These artifacts are obvious on the level of a single peptide structure (Figure 5), where the GHF spectra fail to reproduce features systematically predicted by other methods for wavelengths below 210 nm. However, the performance of both B3LYP and PBE0 improves significantly upon averaging over many structures, for all investigated models. The understanding of such a trend emerges from an in-depth analysis of the surplus states, whose rotatory strengths are either insignificant or behave essentially randomly as a function of geometry. Consequently, the averaging procedure, essential to calculations of CD spectra of flexible molecules, becomes beneficial for the accuracy of TD-DFT. Such improvement is apparent for both PBE0 and B3LYP but is perhaps more significant in the latter case, which ultimately provides a spectrum exhibiting substantial agreement with the main features of its experimentally observed counterpart.

The agreement is especially significant for the amide excitations, which are responsible for the dominant maximum in the CD spectrum of Met_N (Figure 9). The latter is best reproduced by M06-2X and B3LYP, suggesting that these functionals are particularly suitable for modeling this transition type, a conclusion supported by previous B3LYP calculations of helical alanine chains.[20] From this point of view, the amide transitions predicted by CAM-B3LYP and ωB97X-D are blue-shifted, which is interesting from the perspective that this functional nearly quantitatively reproduces the RICC2 results,[53] particularly for amide excitations (final four rows in Table 2). Similar overall conclusions regarding the applicability of TD-DFT functionals were obtained in the case of transition metal complexes.[19]

CONCLUSIONS

We have shown that the TD-DFT approach can be used to calculate the properties necessary to derive CD spectra of flexible peptides. The charge transfer artifacts occurring with some functionals are significantly diminished by the essential process of averaging the spectrum over the entire conformational space. We used the high level RICC2 as a benchmark method to evaluate the performance of various functionals. Despite its complexity, RICC2 is not always capable of providing accurate predictions of excitation energies,[23,41−43] and for certain transition types investigated herein, we also found indirect evidence for non-negligible deviations from experimental values. For the smaller model systems, CAM-B3LYP (along with ωB97X-D) was found to exhibit nearly quantitative agreement with RICC2 for all three transition types and could thus be used as a reasonable indicator of the RICC2 result for the larger system. In that context, the LCFs (CAM-B3LYP and ωB97X-D) showed a less satisfactory agreement with experimental data than PBE0, which was in turn slightly inferior to B3LYP and M06-2X. Thus, when considering the reproduction and understanding of experimental CD spectra, the choice of the functional should be adjusted to the types of transitions expected to dominate.[36] At this point, it may occur that TD-DFT is actually to be preferred over the RICC2 approach. This is not only because of its better agreement with experimental data for certain transition classes but also because it can be conveniently used, even for relatively large molecules, to evaluate the substantial number of conformations required to achieve converged CD spectra for flexible molecules.

ASSOCIATED CONTENT

Supporting Information

Supporting Figures S1−S7 and Supporting Tables S1−S4. This material is available free of charge via the Internet at http://pubs.acs.org.

AUTHOR INFORMATION

Corresponding Authors

*E-mail: David.Smith@irb.hr.
*E-mail: smith@physik.uni-erlangen.de.

Notes

The authors declare no competing financial interest.

ACKNOWLEDGMENTS

This work was financially supported by the EAM Cluster of Excellence at Friedrich Alexander University Erlangen—Nürnberg, the Croatian Ministry of Science and the Croatian Science Foundation under the project CompSoLS-MolFlex. Z.B. acknowledges support from the Elite Network of Bavaria.

REFERENCES

(1) Greenfield, N. J. *Nat. Protoc.* **2007**, *1*, 2876.
(2) Woody, R. W. *Monatsh. Chem.* **2005**, *136*, 347.
(3) Jiang, J.; Abramavicius, D.; Bulheller, B. M.; Hirst, J. D.; Mukamel, S. *J. Phys. Chem. B* **2010**, *114*, 8270.
(4) Abramavicius, D.; Jiang, J.; Bulheller, B. M.; Hirst, J. D.; Mukamel, S. *J. Am. Chem. Soc.* **2010**, *132*, 7769.
(5) Greenfield, N. J. *Anal. Biochem.* **1996**, *235*, 1.
(6) Gopal, R.; Park, J. S.; Seo, C. H.; Park, Y. *Int. J. Mol. Sci.* **2012**, *13*, 3229.
(7) Glättli, A.; Daura, X.; Seebach, D.; van Gunsteren, W. F. *J. Am. Chem. Soc.* **2002**, *124*, 12972.
(8) Brkljača, Z.; Čondić-Jurkić, K.; Smith, A.-S.; Smith, D. M. *J. Chem. Theory Comput.* **2012**, *8*, 1694.
(9) Sanchez, M. L.; Aguilar, M. A.; Olivares del Valle, F. J. *J. Comput. Chem.* **1997**, *18*, 313.
(10) Coutinho, K.; Georg, H. C.; Fonseca, T. L.; Ludwig, V.; Canuto, S. *Chem. Phys. L.* **2007**, *437*, 148.
(11) Maksimenka, K. *Absolute Configuration by Circular Dichroism: Quantum Chemical CD Calculations*, Ph.D. thesis, Julius-Maximilians-Universität Würzburg: Würzburg, Germany, 2010.
(12) Daura, X.; Bakowies, D.; Seebach, D.; Fleischhauer, J.; van Gunsteren, W. F.; Krüger, P. *Eur. Biophys. J.* **2003**, *32*, 661.
(13) Roos, B. O.; Andersson, K.; Fulscher, M. P.; Malmqvist, P. A.; Serrano-Andres, L.; Pierloot, K.; Merchan, M. *Adv. Quantum Chem.* **1996**, *93*, 219.
(14) Grimme, S.; Waletzke, M. *Phys. Chem. Chem. Phys.* **2000**, *2*, 2075.
(15) Krylov, A. *Annu. Rev. Phys. Chem.* **2008**, *59*, 433.
(16) Christiansen, O.; Koch, H.; Jørgensen, P. *Chem. Phys. Lett.* **1995**, *243*, 409.
(17) Warnke, I.; Furche, F. *WIREs Comput. Mol. Sci.* **2012**, *2*, 150.
(18) Autschbach, J.; Jorge, F. E.; Ziegler, T. *Inorg. Chem.* **2003**, *42*, 2867.
(19) Rudolph, M.; Autschbach, J. *J. Phys. Chem. A* **2011**, *115*, 14677.
(20) Kaminský, J.; Kubelka, J.; Bouř, P. *J. Phys. Chem. A* **2011**, *115*, 1734.
(21) Aquino, A. J. A.; Nachtigallova, D.; Hobza, P.; Truhlar, D. G.; Hättig, C.; Lischka, H. *J. Comput. Chem.* **2011**, *32*, 1217.
(22) Wakai, A.; Fukasawa, H.; Yang, C.; Mori, T.; Inoue, Y. *J. Am. Chem. Soc.* **2012**, *134*, 4990.
(23) Jacquemin, D.; Wathelet, V.; Perpète, E. A.; Adamo, C. *J. Chem. Theory Comput.* **2009**, *5*, 2420.
(24) Kuritz, N.; Stein, T.; Baer, R.; Kronik, L. *J. Chem. Theory Comput.* **2011**, *7*, 2408.
(25) Peach, M. J. G.; Benfield, P.; Helgaker, T.; Tozer, D. J. *J. Chem. Phys.* **2008**, *128*, 044118.
(26) Li, R.; Zheng, J.; Truhlar, D. G. *Phys. Chem. Chem. Phys.* **2010**, *12*, 12697.
(27) Tozer, D. J.; Amos, R. D.; Handy, N. C.; Roos, B. O.; Serrano-Andrés, L. *Mol. Phys.* **1999**, *97*, 859.
(28) Yanai, T.; Tew, D. P.; Handy, N. C. *Chem. Phys. Lett.* **2004**, *393*, 51.
(29) Chai, J.-D.; Head-Gordon, M. *Phys. Chem. Chem. Phys.* **2008**, *10*, 6615.
(30) Zhao, Y.; Truhlar, D. G. *Theor. Chem. Acc.* **2008**, *120*, 215.
(31) Charaf-Eddin, A.; Planchat, A.; Mennucci, B.; Adamo, C.; Jacquemin, D. *J. Chem. Theory Comput.* **2013**, *9*, 2749.
(32) Becke, A. D. *J. Chem. Phys.* **1993**, *98*, 5648.
(33) Ernzerhof, M.; Scuseria, G. E. *J. Chem. Phys.* **1999**, *110*, 5029.
(34) Jamorski, C.; Foresman, J. B.; Thilgen, C.; Lüthi, H.-P. *J. Chem. Phys.* **2002**, *116*, 8761.
(35) Guido, C. A.; Knecht, S.; Kongsted, J.; Mennucci, B. *J. Chem. Theory Comput.* **2013**, *9*, 2209.
(36) Laurent, A. D.; Jacquemin, D. *Int. J. Quantum Chem.* **2013**, *113*, 2019.
(37) Grimme, S. J. *Chem. Phys.* **2006**, *124*, 034108.
(38) Goerigk, L.; Grimme, S. *J. Phys. Chem. A* **2009**, *113*, 767.
(39) Hättig, C.; Weigend, F. *J. Chem. Phys.* **2000**, *113*, 5154.
(40) Hättig, C.; Köhn, A. *J. Chem. Phys.* **2002**, *117*, 6939.
(41) Silva-Junior, M. R.; Schreiber, M.; Sauer, S. P. A.; Thiel, W. *J. Chem. Phys.* **2008**, *129*, 104103.
(42) Schreiber, M.; Silva-Junior, M. R.; Sauer, S. P. A.; Thiel, W. *J. Chem. Phys.* **2008**, *128*, 134110.
(43) Crawford, T. D.; Stephens, P. J. *J. Phys. Chem. A* **2008**, *112*, 1339.
(44) Gredičak, M.; Supek, F.; Kralj, M.; Majer, Z.; Hollosi, M.; Šmuc, T.; Mlinarić-Majerski, K.; Horvat, Š. *Amino Acids* **2009**, *38*, 1185.
(45) Humphrey, W.; Dalke, A.; Schulten, K. *J. Mol. Graphics* **1996**, *14*, 33.
(46) Duan, Y.; Wu, C.; Chowdhury, S.; Lee, M. C.; Xiong, G.; Zhang, W.; Yang, R.; Cieplak, P.; Luo, R.; Lee, T.; Caldwell, J. W.; Wang, J.; Kollman, P. A. *J. Comput. Chem.* **2003**, *23*, 1999.
(47) Case, D. A.; Darden, T. A.; Cheatham, T. E., III; Simmerling, C. L.; Wang, J.; Duke, R. E.; Luo, R.; Crowley, M.; Walker, R. C.; Zhang, W.; Merz, K. M.; Wang, B.; Hayik, S.; Roitberg, A.; Seabra, G.; Kolossváry, I.; Wong, K. F.; Paesani, F.; Vanicek, J.; Wu, X.; Brozell, S. R.; Steinbrecher, T.; Gohlke, H.; Yang, L.; Tan, C.; Mongan, J.; Hornak, V.; Cui, G.; Mathews, D. H.; Seetin, M. G.; Sagui, C.; Babin, V.; Kollman, P. A. *AMBER 10*; University of California: San Francisco, CA, 2008.
(48) Dupradeau, F.-Y.; Cézard, C.; Lelong, R.; Stanislawiak, E.; Pecher, J.; Delepine, J. C.; Cieplak, P. *Nucleic Acids Res.* **2008**, *36*, 360.
(49) *TURBOMOLE*, V6.3; University of Karlsruhe; Forschungszentrum Karlsruhe GmbH: Karlsruhe, Germany, 1989−2007; TURBOMOLE GmbH: Karlsruhe, Germany, 2011.
(50) Dunning, T. H. *J. Chem. Phys.* **1989**, *90*, 1007.
(51) Frisch, M. J.; Trucks, G. W.; Schlegel, H. B.; Scuseria, G. E.; Robb, M. A.; Cheeseman, J. R.; Scalmani, G.; Barone, V.; Mennucci, B.; Petersson, G. A.; Nakatsuji, H.; Caricato, M.; Li, X.; Hratchian, H. P.; Izmaylov, A. F.; Bloino, J.; Zheng, G.; Sonnenberg, J. L.; Hada, M.; Ehara, M.; Toyota, K.; Fukuda, R.; Hasegawa, J.; Ishida, M.; Nakajima, T.; Honda, Y.; Kitao, O.; Nakai, H.; Vreven, T.; Montgomery, J. A., Jr.; Peralta, J. E.; Ogliaro, F.; Bearpark, M.; Heyd, J. J.; Brothers, E.; Kudin, K. N.; Staroverov, V. N.; Kobayashi, R.; Normand, J.; Raghavachari, K.; Rendell, A.; Burant, J. C.; Iyengar, S. S.; Tomasi, J.; Cossi, M.; Rega, N.; Millam, N. J.; Klene, M.; Knox, J. E.; Cross, J. B.; Bakken, V.; Adamo, C.; Jaramillo, J.; Gomperts, R.; Stratmann, R. E.; Yazyev, O.; Austin, A. J.; Cammi, R.; Pomelli, C.; Ochterski, J. W.; Martin, R. L.; Morokuma, K.; Zakrzewski, V. G.; Voth, G. A.; Salvador, P.; Dannenberg, J. J.; Dapprich, S.; Daniels, A. D.; Farkas, Ö.; Foresman, J. B.; Ortiz, J. V.; Cioslowski, J.; Fox, D. J. *Gaussian 09*, revision A.02; Gaussian, Inc.: Wallingford, CT, 2009.
(52) Zhang, L.; Peslherbe, G. H.; Muchall, H. M. *Photochem. Photobiol.* **2006**, *82*, 324.
(53) *Circular Dichroism: Principles and Applications*, 2nd ed.; Berova, N., Nakanishi, K., Woody, R. W., Eds.; Wiley-VCH: New York, 2000; p 75.
(54) Parac, M.; Grimme, S. *J. Phys. Chem. A* **2002**, *106*, 6844.